

January 01, 2008

A parameter study of separation modes of adhering microcontacts

Yan Du

Northeastern University - MicroFabrication Laboratory

George G. Adams

Northeastern University - MicroFabrication Laboratory

Nicol E. McGruer

Northeastern University - MicroFabrication Laboratory

Izhak Etsion

Technion-Israel Institute of Technology - Dept. of Mechanical Engineering

Recommended Citation

Du, Yan; Adams, George G.; McGruer, Nicol E.; and Etsion, Izhak, "A parameter study of separation modes of adhering microcontacts" (2008). *Center for High-Rate Nanomanufacturing Publications*. Paper 4. <http://hdl.handle.net/2047/d20000888>

A parameter study of separation modes of adhering microcontacts

Yan Du,¹ George G. Adams,^{1,a)} Nicol E. McGruer,¹ and Izhak Etsion²

¹MicroFabrication Laboratory, Northeastern University, Boston, Massachusetts 02115, USA

²Department of Mechanical Engineering, Technion-Israel Institute of Technology, Haifa 32000, Israel

(Received 21 August 2007; accepted 17 December 2007; published online 19 March 2008)

A finite element model was developed to study adhesion of elastic-plastic microcontacts in a previous investigation. An interesting result was the identification of two distinct separation modes, i.e. brittle and ductile separation. In the current study, that model is used to conduct a series of simulations to determine the influence of four nondimensional parameters (including the maximum load parameter) on the contact and on the separation modes. The results show that the parameter S (the ratio of the theoretical stress to the hardness) and δ_f/δ_c (representing the loading level) are the most important. Smaller S can only lead to brittle separation, while larger S can cause either separation mode depending on δ_f/δ_c . Ductile separation is more likely to occur at smaller δ_f/δ_c and brittle separation at greater δ_f/δ_c . The transition between the two separation modes occurs at about $S=1.2$ (for $\delta_f/\delta_c=30$) which corresponds to the theoretical stress for adhesion being 20% greater than the hardness. This result is qualitatively similar to the existing simplified analytical models, in that the adhesion energy, the hardness, and the loading level play important roles in the occurrence of ductile separation. However, there are important quantitative differences. Comparisons are also made with molecular dynamics simulations of a contact and with a fracture mechanics model of crack propagation. © 2008 American Institute of Physics. [DOI: 10.1063/1.2874434]

I. INTRODUCTION

In the contact of two solids, plastic deformation leads to permanent changes in the contact topography. It can be initiated by the force applied to the contact by adhesion alone even under zero external force or by a combination of load and adhesion.¹⁻⁴ The plastic deformation produced by adhesion alters the local separation of the surfaces which in turn affects the adhesion force. Understanding the mechanics of contacts, which includes both the effects of adhesion and plasticity, is a complex problem which is still not well understood. However, developing such an understanding is especially important due to the rapid development of devices at the micron scale or smaller.

This paper is concerned with the contacts which occur in a variety of microscale applications, most notably in a microswitch. Such a contact can be simply represented as a hemisphere, with a radius R , in adhesive contact with a rigid flat surface, as shown in Fig. 1. The contact radius under the external load F_e is denoted by a . The interference δ is defined as the distance between the summit of the original sphere (dashed line) and that of the loaded sphere (solid line); it is positive when the sphere is in compression. The contact force F is the sum of the external force F_e and the adhesion force F_s , i.e.,

$$F = F_e + F_s, \tag{1}$$

The final (maximum) values of the external force, contact radius, and interference are denoted by F_f , a_f , and δ_f , respectively.

The continuum mechanics analysis of elastic contact

with adhesion is now well understood. A very important dimensionless parameter was introduced by Tabor⁵ as

$$\mu = \left(\frac{R\Delta\gamma^2}{E^*Z_0^3} \right)^{1/3} \tag{2}$$

for the contact of an elastic sphere with a rigid and flat surface. In Eq. (2), R is the radius of the sphere, E^* is the effective Young's modulus given by $E/(1-\nu^2)$, in which E is Young's modulus and ν is the Poisson ratio, $\Delta\gamma$ is the adhesion energy, and Z_0 is the equilibrium distance between the surfaces. Generally for $\mu > 3$, the Johnson-Kendall-Roberts (JKR) model⁶ is applicable, and for $\mu < 0.1$, the Derjaguin-Muller-Toporov (DMT) model⁷ is appropriate. Maugis gave an analytical solution under simplified assumptions to realize a smooth transition from the JKR to the DMT model.⁸ The adherence force (pull-off force) required to separate the contact is⁸

$$F_{adh} = \alpha\pi\Delta\gamma R, \tag{3}$$

in which the coefficient α varies from $\frac{3}{2}$ to 2 as the Tabor parameter μ decreases from the JKR to the DMT region. All

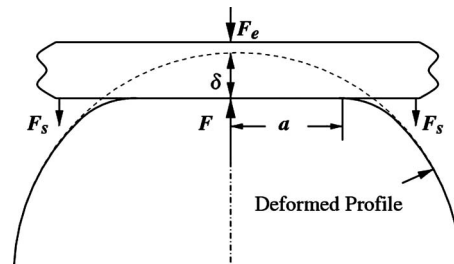


FIG. 1. A single asperity contact with adhesion between a hemisphere and a rigid flat.

^{a)}Electronic mail: adams@coe.neu.edu.

the above models are only applicable for elastic contact.

When the contacting bodies experience pressure beyond the elastic limit, the contact is elastoplastic (some material is plastic, while the surrounding material is elastic) or fully plastic (the entire contact area undergoes plastic deformation with the contact pressure equal to the hardness H , which is related to the yield strength by $H=2.8\sigma_Y$). The critical interference for the initiation of yielding without adhesion (e.g., Chang *et al.*⁹) is

$$\delta_c = \left(\frac{\pi K_H H}{2E^*} \right)^2 R. \quad (4)$$

In Eq. (4), the hardness coefficient is given by $K_H=0.454+0.41\nu$. The critical contact radius a_c and the critical contact force F_c corresponding to the critical interference are found from the well-known equations for Hertz contact,¹⁰ i.e.,

$$a_c = (\delta_c R)^{1/2}, \quad (5)$$

$$F_c = \left(\frac{2}{3} \right) K_H H \pi \delta_c R. \quad (6)$$

A simple analytical model of elastoplastic and fully plastic deformation with adhesion was developed by Majumder *et al.*¹¹ for use in a microswitch using techniques from Maugis and Pollock³ and Johnson.¹⁰ Plastic loading is irreversible, and some permanent deformation remains after unloading. If the deformed sphere recovers elastically, its residual radius of curvature R_{res} can be estimated from the Hertz relation,

$$R_{\text{res}} = \frac{4a_f E^*}{3\pi p_m} = \frac{4E^* F_f^{1/2}}{3(\pi p_m)^{3/2}}. \quad (7)$$

In Eq. (7), p_m is the mean pressure at the maximum loading. It is smaller than H for elastoplastic deformation and equal to H for fully plastic deformation. Replacing R by R_{res} in Eq. (3) gives an adherence force,

$$F_{\text{adh}} = \alpha \pi \Delta \gamma R_{\text{res}} = \frac{4\alpha \Delta \gamma E^* F_f^{1/2}}{3(\pi p_m^3)^{1/2}}. \quad (8)$$

Thus, for a fully plastic contact, the adherence force varies as the square root of the maximum applied load.

Unfortunately, it is very difficult for an analytical model to adequately predict the complicated phenomena which occurs in a plastically deforming adhesive contact because of the many simplifying assumptions needed in order to obtain a solution. It is both more accurate and straightforward to solve such problems using numerical methods. In our recent work, a finite element model (FEM) was developed to study adhesion in an elastic-plastic microcontact.¹ That model differs from previous FEMs [e.g., the Kogut–Etsion (KE) model without¹² and with¹³ adhesion] in that it includes the coupled effects of adhesion on the deformation and stress fields, thus making it applicable to a wide range of material properties. Simulations were performed in Ref. 1 during a single load-unload cycle at four different maximum loading levels for both ruthenium (Ru) and gold (Au) contacts. These metals are two popular materials used in microelectromechanical systems (MEMS) switches and are expected to show distinguishable contact properties.²

Interestingly, during unloading, two distinct separation modes, i.e., brittle separation and ductile separation, were observed in Ref. 1 for Ru and Au, respectively. The characteristics of ductile separation can be summarized by the following four characteristics. First, the contact radius decreases slowly and stepwise before it suddenly separates, typically at a significant fraction of the maximum contact radius. In a brittle separation, the contact radius decreases steadily to a small value before separating. Second, the hemispherical bump is stretched significantly during separation due to plastic deformation; it is this behavior which best characterizes ductile separation. Third, the adherence force for a ductile separation is much larger than for a brittle separation. Fourth, a neck is sometimes formed during the ductile separation, but not for a brittle separation. It is noted that Johnson¹⁴ and Maugis and Pollock³ (MP) mentioned brittle separation and ductile separation as early as 1976 and 1984, respectively. However, although 30 years have passed, the accurate criteria to distinguish between these two modes of adhesive separation are still not clear.

The MP model³ is an approximate analytical treatment of plastic deformation in an adhesive contact. For elastic loading, it is the same as the JKR model. For either elastoplastic or fully plastic loading, the radius of curvature of the deformable body in the contact region changes. Unloading is assumed to be elastic with the modified radius of curvature until separation occurs. If the tensile stress becomes equal to the hardness H , a ductile separation is said to occur. However, the ductile separation is not itself modeled; it is only the assumed completely elastic unloading prior to the ductile separation which is treated. Another possibility during unloading is either of two different brittle separation modes. The occurrence of each of these three modes depends on the maximum contact radius during loading and the material properties. An interesting and somewhat counterintuitive result of the MP model is that ductile separation is more likely to occur at low loads, provided that the load is large enough for the initiation of some plastic deformation during loading. The criteria for the occurrence of ductile separation is

$$a_f < \frac{8E^* \Delta \gamma}{\pi(H + p_m)^2}. \quad (9)$$

Mesarovic and Johnson (MJ) used a combination of finite elements and an analytical method under the assumption that the contact pressure at the end of loading is uniform.¹⁵ The near uniformity of the contact pressure is shown to occur well before the onset of full plasticity. They defined a nondimensional parameter given by

$$S' = \frac{\Delta \gamma}{Z_0 p_m}. \quad (10)$$

From Eq. (10), S' is approximately equal to the theoretical stress (the maximum Lennard-Jones stress between two parallel surfaces) divided by the mean contact pressure at the maximum loading level. Note that because the mean pressure cannot be greater than the hardness, S' cannot be less than the ratio of the theoretical stress to the hardness. A second parameter in Ref. 15 is

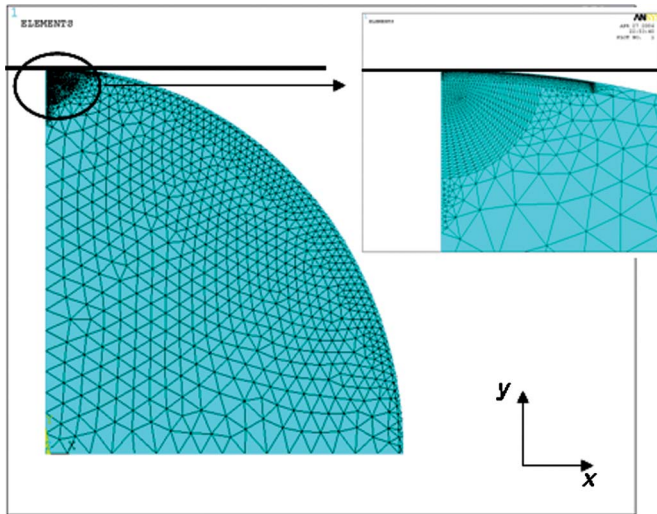


FIG. 2. (Color online) Finite element mesh used for the ANSYS® simulation of contact with adhesion.

$$\chi = \frac{\pi}{2\pi - 4} \frac{\Delta\gamma E^*}{p_m^2 a_f}, \quad (11)$$

which can be interpreted as the ratio of the adhesive energy to the elastic energy stored in the recovered hemisphere. A decohesion map was presented, whereby the parameter space (χ, S') was divided into the regions where decohesion is governed by different physical processes. In all cases, it was assumed that the unloading is elastic up until the point of separation. When $S' < 1$, the separation is elastic, while for $S' > 1$, yielding results during separation, and is expected to be widespread.

Another approach to this adhesion problem is through the use of molecular dynamics (MD) simulations. Early work was done by Landman *et al.* who observed the formation and elongation of a connective neck upon separation between a nickel tip and a gold surface.¹⁶ More recent investigations were made by Song and Srolovitz¹⁷ for Au nanocontacts, and by Yong *et al.* for NaCl.¹⁸ In Ref. 17, the radius of curvature of the Au asperity is approximately 3 nm. The adhesion energy was varied, while leaving the other properties unchanged. Three different separation modes were identified in the order of increasing adhesion energy—elastic separation, plastic interface separation, and plastic noninterface separation (accompanied by material transfer). The residual morphology shows a neck profile (ductile separation) which was first visible at an adhesion energy equal to 0.61 J/m². Certainly, the MD simulations are applicable to study contacts at the atomic scale, while we are using a continuum model to study contacts at microscale.

Rice and Thomson also made a significant related contribution by predicting the conditions for separation modes of cracks using fracture mechanics.^{19,20} Brittle versus ductile behavior is described as a competition between Griffith cleavage and plastic shear (dislocation nucleation) at a crack tip under plane strain conditions. The requirement for ductile fracture to occur under mode I loading (i.e., a crack in pure tension) is

$$\frac{\gamma_s}{\gamma_{us}} > 9.1(\text{fcc}) \text{ or } \frac{\gamma_s}{\gamma_{us}} > 6.3(\text{bcc}). \quad (12)$$

Using this approach, we calculate the critical surface energy for gold, a fcc metal, for the ductile separation to be about 0.88 J/m² based on an unstable stacking fault energy $\gamma_{us} = 0.14$ J/m² given in Ref. 20 by the Frenkel model. In a brittle fracture problem, $\Delta\gamma$ is twice γ_s but in an adhesion problem of identical materials, surface contamination will cause $\Delta\gamma$ to be less than twice γ_s . Nonetheless, in both cases, greater adhesion energy tends to cause ductile separation for the same material and loading conditions.

As can be seen from the foregoing discussion, there exists a wide variety of work devoted to ductile and brittle separation modes. However, there is still a lack of general results to apply to microscale or nanoscale adhesive contacts. Understanding the unloading of a contact is very important because failure mechanisms in, for example, a microswitch can be attributed to ductile separation resulting from too high an adherence force.^{2,21} In this paper, we use the previously developed FEM (Ref. 1) to study adhesion of elastic-plastic microcontacts with the objective of determining the influence of the various parameters on the separation modes of these adhesive contacts.

II. THE DIMENSIONLESS CONTACT PARAMETERS

The first dimensionless parameter is defined by

$$S = \frac{\Delta\gamma}{Z_0 H}. \quad (13)$$

This parameter S is the ratio of the theoretical stress due to adhesion to the hardness. It is similar to S' defined by Eq. (10) except that the mean contact pressure is replaced by the hardness. Note that for fully plastic deformation, $p_m = H$ in which case $S = S'$.

The second parameter is E/σ_Y which is the ratio of Young's modulus to the yield strength. It was found in Ref. 22 that, without adhesion, this parameter does not affect the loading curves which were plotted using dimensionless parameters. However, during unloading, the residual radius of curvature R_{res} does depend on E/σ_Y which further affects the adhesion force. From Ref. 22, the adherence force is equal to $2\pi\Delta\gamma R_{\text{res}}$ for DMT behavior. More discussion of the role of R_{res} is presented later.

The third parameter is the Tabor parameter defined in Eq. (2) for elastic contact. Note that if the unloading is elastic, an effective μ increases with the plastic deformation incurred during loading due to the increase of the residual radius of curvature R_{res} . For elastic unloading, larger μ decreases the adherence force, but larger R also corresponds to a larger adherence force. The effect of larger R dominates that of larger μ .

The load level is defined by the dimensionless interference as δ_f/δ_c which is used to study the effect of different loading interferences on adhesion during unloading. Note that both the MP and MJ models predict that the occurrence of ductile separation is related to the load level.

TABLE I. Mechanical conversion factors for μmks to new units used in ANSYS®.

Mechanical parameter	μmks unit	Dimension	Multiply by this number	To obtain new unit	Dimension
Length	μm	μm	$1/b$	$b \mu\text{m}$	$b \mu\text{m}$
Pressure	MPa	$\text{kg}/(\mu\text{m})(\text{s})^2$	b	$(1/b)\text{MPa}$	$\text{kg}/(b \mu\text{m})(\text{s})^2$
Force	μN	$(\text{kg})/(\mu\text{m})(\text{s})^2$	$1/b$	$b \mu\text{N}$	$(\text{kg})/(b \mu\text{m})(\text{s})^2$

III. CONTINUUM FINITE ELEMENT MODEL

The adhesive contact model is described in detail in Ref. 1; here, we review some of the most relevant aspects of that model. Figure 2 shows the meshed FEM using ANSYS®. The contact is made between a deformable hemispheric bump, with radius of curvature R , and a rigid flat surface. The displacement or the interference δ of the top flat surface is the controlled loading variable. It is defined as the vertical distance between the top flat and the summit of the undeformed sphere. Negative interference means the top flat is above the undeformed hemisphere summit. The adhesive interaction is represented by the Lennard-Jones potential between two parallel surfaces. The angle between the normal and vertical directions is small enough to neglect this difference. The deformation of the sphere under the combined effects of displacement and attractive stresses at each displacement of the flat is found by an iterative procedure.

In Ref. 1, contacts of Au and Ru were studied with a hemisphere radius equal to 1 and 4 μm , respectively. The two FEMs with different sizes were meshed in the same manner such that the surface of the sphere was covered by a thin layer of fine elements with a size of 3 nm in order to resolve the effect of adhesion. The inner sphere was divided into two different mesh density zones, in which the zone closer to the apex had the finer mesh. The material of the sphere was assumed to have linear hardening characterized by a tangent modulus E_T equal to 2% of Young's modulus. This value is within the range of values often observed.²³ The von Mises yield criterion was used to detect the local transition from elastic to plastic deformation.

The use of continuum theory requires that the atomic spacing be much less than any significant dimension of the body. Although the minimum finite element size of 3 nm is much greater than the atomic spacing of Au or Ru (less than 0.3 nm), it is not the size of the element *per se* which is critical. A finite element solution converges to the analytical solution only in the limit as the element size shrinks to zero. The fact that solutions are routinely obtained for much larger element size is due to a trade-off between computational time and acceptable accuracy. It is noted that a closed-form

solution of a continuum problem has an infinitesimal element size.

IV. RESULTS AND DISCUSSION

A. The choice of dimensionless variables

To study the importance of each of the parameters, four groups of simulations were performed. In each group, one of the parameters was varied while keeping the other three constant. In order to effectively show the characteristics of ductile and brittle separation from these cases with different material properties, appropriate dimensionless variables are chosen, i.e., dimensionless interference δ/δ_f , dimensionless contact radius a/a_f , and dimensionless external force F_e/F_f . The quantities δ_f , a_f , and F_f are the interference, contact radius, and external force, respectively, at the final maximum interference during loading.

First, we analyze the adherence force. As a basis for comparison, consider the curve fit to the finite element simulations for R_{res} with plastic deformation given by Etsion, Kligerman, and Kadin (EKK),²²

$$R_{\text{res}}^{\text{EKK}} = R \left[1 + 1.275 \left(\frac{E}{\sigma_Y} \right)^{-0.216} (\delta_f/\delta_c - 1) \right]. \quad (14)$$

Note that here R_{res} is the residual radius of curvature at the summit of the deformed and fully unloaded sphere. This value is found to be greater at the summit than at other radial positions, indicating that the sphere has been flattened more at its apex than elsewhere. Although the EKK model was built without adhesion, it can still be applicable for the DMT type of adhesion since the DMT model neglects the effect of adhesion on deformation. The adherence force is then $F_{\text{adh}}^{\text{EKK}} = 2\pi\Delta\gamma R_{\text{res}}^{\text{EKK}}$. The ratio of the contact force F^{KE} to the critical contact force F_c is a function only of δ_f/δ_c , given by the KE model,¹²

$$\frac{F^{\text{KE}}}{F_c} = \begin{cases} 1.03(\delta_f/\delta_c)^{1.425} & \text{for } 1 \leq \delta_f/\delta_c \leq 6 \\ 1.40(\delta_f/\delta_c)^{1.263} & \text{for } 6 \leq \delta_f/\delta_c \leq 110. \end{cases} \quad (15)$$

So the adherence force predicted by the combination of the EKK model and the KE model is

TABLE II. Material properties for the study of the impact of parameter S (S varies from 0.6 to 2.9, $E/\sigma_Y = 120$, $\mu = 1.60$, and $\delta_f/\delta_c = 30$).

Case	R (μm)	E (GPa)	ν	σ_Y (GPa)	Z_0 (nm)	$\Delta\gamma$ (J/m ²)	δ_c (nm)	S
1	4	410	0.3	3.42	0.169	1	1.48	0.6
2	1.3	233	0.3	1.94	0.169	1	0.47	1.0
3	1.5	54.7	0.42	0.46	0.184	0.28	0.52	1.2
4	0.2	418	0.42	3.5	0.169	4.8	0.07	2.9

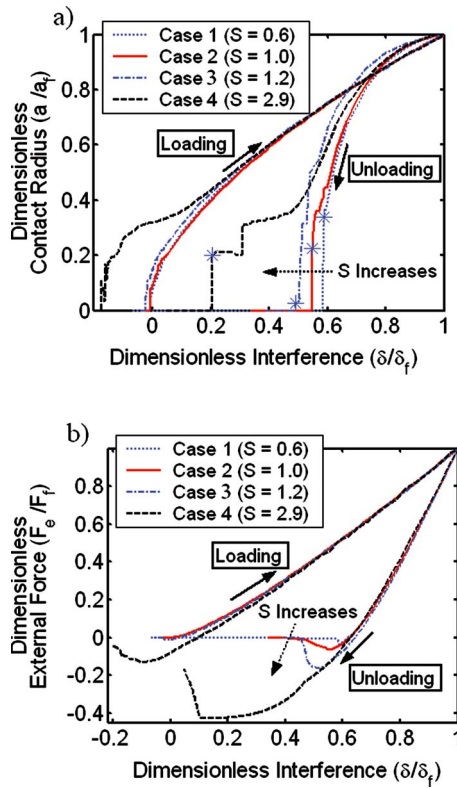


FIG. 3. (Color online) Dimensionless contact radius vs dimensionless interference (a) and dimensionless external force vs dimensionless interference (b) for a single load/unload cycle. The material properties and geometry are given in Table II (S varies from 0.6 to 2.9, $E/\sigma_Y=120$, $\mu=1.60$, and $\delta_f/\delta_c=30$).

$$\frac{F_{adh}}{F_f} = \frac{2\pi\Delta\gamma R_{res}^{EKK}}{F^{KE}}$$

$$= \frac{12(1-\nu^2)^2}{K_H^3\pi^2} \left[\frac{1 + 1.275\left(\frac{E}{\sigma_Y}\right)^{-0.216} (\delta_f/\delta_c - 1)}{[1.03(\delta_f/\delta_c)^{1.425}] \text{ or } [1.4(\delta_f/\delta_c)^{1.263}]} \right] S^3, \quad (16)$$

which depends only on the four dimensionless parameters [although in Eq. (16), S/μ can be interpreted as a single parameter]. The effect of Poisson's ratio is not considered. Because the KE model does not include the effect of adhesion on deformation, it is incapable of predicting ductile separation. It was found in Ref. 1 that the difference of the adherence forces between our model and the KE model is within the range of 10%–32% for Ru (brittle separation) and Au cases (ductile separation) except for the smallest loading interference for Au. The maximum external force for a given interference is also consistent with F^{KE} for large loading be-

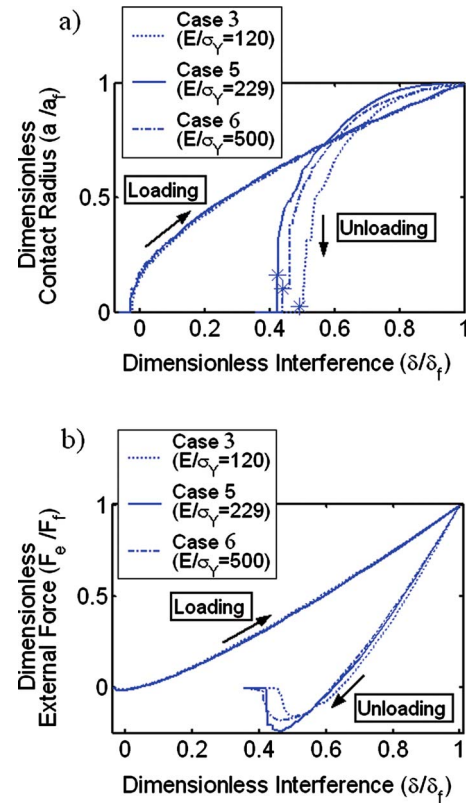


FIG. 4. (Color online) Dimensionless contact radius vs dimensionless interference (a) and dimensionless external force vs dimensionless interference (b) for a single load/unload cycle. The material properties and geometry are given in Table III (E/σ_Y varies from 120 to 500, $S=1.2$, $\mu=1.60$, and $\delta_f/\delta_c=30$).

cause for large loads the adhesion force is small in comparison. Although Eq. (16) alone cannot be used to identify the separation modes, it may be appropriate for brittle separation and to provide qualitative insight into the more general unloading problem.

It was also found in Ref. 1 that the value of the interference at which separation occurs is another important indication of ductile separation. If the separation is brittle, then the sphere is not stretched significantly due to adhesion and the residual interference δ_{res} after unloading is close to the residual interference caused without the effect of adhesion. That value is only dependent on δ_f/δ_c and can be obtained using the curve fit from the EKK model. For example, from the EKK model $\delta_{res}/\delta_f=0.555$ for $\delta_f/\delta_c=30$, and $\delta_{res}/\delta_f=0.137$ for $\delta_f/\delta_c=2.94$ which are two typical loading levels we used for the simulations. From Ref. 1, δ_{res}/δ_f is equal to 0.5867 and 0.0655, respectively, for brittle separation of Ru, and 0.1674 and -2.2558 for ductile separation of Au. In the

TABLE III. Material properties for the study of the impact of parameter E/σ_Y (E/σ_Y varies from 120 to 500, $S=120$, $\mu=1.60$, and $\delta_f/\delta_c=30$).

Case	R (μm)	E (GPa)	ν	σ_Y (GPa)	Z_0 (nm)	$\Delta\gamma$ (J/m ²)	δ_c (nm)	E/σ_Y
3	1.5	54.7	0.42	0.46	0.184	0.28	0.52	120
5	4	410	0.3	1.79	0.169	1	0.41	229
6	20.9	85.9	0.3	0.17	0.184	0.1	0.44	500

TABLE IV. Material properties for the study of the impact of parameter μ (μ varies from 1.60 to 3.50, $S=1.2$, $E/\sigma_Y=120$, and $\delta_f/\delta_c=30$).

Case	R (μm)	E (GPa)	ν	σ_Y (GPa)	Z_0 (nm)	$\Delta\gamma$ (J/m ²)	δ_c (nm)	μ
3	1.5	54.7	0.42	0.46	0.184	0.28	0.52	1.60
7	6	54.7	0.42	0.46	0.184	0.28	2.17	2.57
8	15	54.7	0.42	0.46	0.184	0.28	5.46	3.50

following work, the amount of plastic stretch is the main criterion to identify the two separation modes. It needs to be mentioned that the definition of ductile separation by the MP and MJ models is that there is a sudden transition from elastic unloading to an expected fully plastic separation. In neither model is the plastic separation itself included in the model. In our work, the unloading is allowed to be elastic and/or plastic as dictated by the results of the simulation. Ductile separation is defined as occurring when considerable stretch occurs during unloading.

B. Equivalent set of units

Many simulations with different combinations of material properties and dimensions are needed to study the effect of the four dimensionless parameters. It is impractical and inefficient to rebuild each model with a different hemisphere size and remesh it accordingly. Fortunately, we can use any consistent system of units provided that we ensure that the units are consistent. For example, in MEMS, it is convenient to set up problems in μmks units instead of the standard mks units. To make use of the existing two models with preset radii of 4 and 1 (arbitrary units), conversion factors in Table I are used to mks units to a new set of units. Specifically, when length is multiplied by a factor of $1/b$ and force by $1/b$, then pressure is multiplied by b accordingly. It is noted that the parameters S , E/σ_Y , μ , and δ_f/δ_c are dimensionless, and so are constant under this conversion. For example, if we use the model with a radius of 4 and want $S=1$, $E/\sigma_Y=120$, and $\mu=1.6$, we can get the corresponding values for $E=75419$, $\Delta\gamma=1$, $\sigma_Y=628.5$, and $Z_0=0.0005219$ by using Eqs. (2) and (13). The units for those numbers are the new units listed in the fifth column of Table I. Those numbers are not necessarily unique. In reality, Z_0 is a constant number, which is 0.169 nm for Ru and 0.184 nm for Au.¹ The validity of the above conversion of units was tested in simulations and showed virtually identical results.

With the above unit conversion method, we can design simulations more effectively. For ease of understanding, the numbers listed in the following tables have been converted to the real material properties and dimensions instead of those entered into ANSYS®.

C. Influence of S on the separation modes

The material properties and dimensions listed in Table II were chosen to study the influence of the parameter S on the separation modes. Two maximum loading levels ($\delta_f/\delta_c=30$ and $\delta_f/\delta_c=2.94$) were chosen while keeping the other two parameters constant ($E/\sigma_Y=120$ and $\mu=1.60$).

All the simulations experience a single cycle of loading and unloading. For the load level of $\delta_f/\delta_c=30$, it can be seen in Fig. 3(a) that the *loading* curves for contact radius versus interference show little variation with S , except for a combination of large S and small loading in which a significant jump into contact occurs. However, the *unloading* curves show a significant dependence on S . The stars (*) mark the contact radii immediately before separation. A gradual change of separation modes from brittle to ductile can be seen with the increase of S . The unloading curves for $S \leq 1.2$ are relatively smooth, while for large S , the contact radii decrease stepwise during unloading. The curve for $S=1.2$ represents the approximate transition between these two cases. Another phenomenon characterized by $S > 1.2$ is that the hemispherical bump is stretched considerably due to the plastic deformation during separation. The dimensionless interference upon separation for $S=2.9$ is equal to 0.2 which is significantly less than the 0.555 value calculated earlier from the EKK model.

Figure 3(b) gives the dimensionless external force versus interference. The negative peak represents the adherence

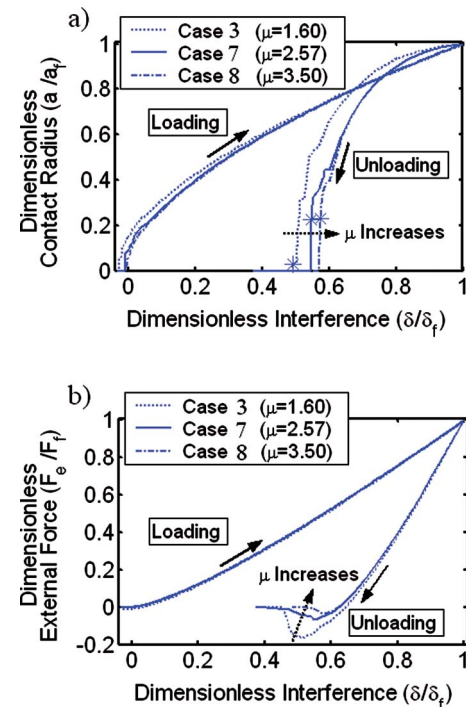


FIG. 5. (Color online) Dimensionless contact radius vs dimensionless interference (a) and dimensionless external force vs dimensionless interference (b) for a single load/unload cycle. The material properties and geometry are given in Table IV (μ varies from 1.60 to 3.50, $S=1.2$, $E/\sigma_Y=120$, and $\delta_f/\delta_c=30$).

TABLE V. Material properties for the study of the impact of parameter δ_f/δ_c (δ_f/δ_c varies from 2.58 to 30).

Case	S	E/σ_Y	μ	δ_f/δ_c			
1	0.6	120	1.60	2.94	10	20	30
3	1.2	120	1.60	2.94	30
6	1.2	500	1.60	2.94	30

force needed to separate the bump from the flat surface. Its magnitude generally increases with an increase of S as also expected by Eq. (16). By taking the ratios of the adherence forces obtained from our simulations with those calculated from Eq. (16), the ratios of 0.96, 0.73, 0.84, and 0.16 are obtained, respectively, for cases 1–4. We can see that the results are close for cases 1–3, but a large difference is obtained for case 4. Let us recall that R_{res} in Eq. (16) is the residual radius of curvature at the summit of the fully unloaded sphere without adhesion which is flattened more at its apex than elsewhere.²² The large discrepancy obtained for case 4 further demonstrates that the residual radius of curvature in our simulation is significantly changed due to large S . The separation mode has changed to ductile and therefore Eq. (16) is no longer applicable. Ductile separation causes the sphere to stretch during unloading, thereby reducing its radius of curvature. Hence, the adherence force is reduced from that expected by Eq. (16), but is still greater than for a brittle separation.

The transition from brittle separation to ductile separation for $\delta_f/\delta_c=30$ is at $S=1.2$. That this ratio of the peak adhesive stress to the hardness needs to be greater than unity is due in part to the greater nonuniformity in the stress field during unloading than during loading. It is also because 2% strain hardening is used for the simulation and thus the effective hardness is greater during unloading.

Another group of simulations are performed for small loading $\delta_f/\delta_c=2.94$ for the cases in Table II. The results are not presented here since they are very similar to those of the above large loading case in that the magnitude of the adherence force increases with an increase of S and the transition between the separation modes occurs at about $S=1.0$, which is smaller than for large loading. At $S=1.2$, the ductile behavior is much more obvious than for large loading. Again, it is emphasized that the transition between brittle and ductile separation is gradual. That lower S for the brittle-to-ductile transition is no doubt due in part to the reduced strain hardening during loading.

It is mentioned earlier in this paper that the onset of ductile separation for Au obtained by MD simulations¹⁷ is at an adhesion energy equal to 0.61 J/m^2 . To compare that model with ours, we take typical values of $Z_0=0.184 \text{ nm}$ and $H=2 \text{ GPa}$ for Au in Eq. (13). Note that the radius of curvature R does not affect S in Eq. (13). The FEM gives the criterion of $\Delta\gamma>0.44 \text{ J/m}^2$ for ductile separation showing reasonable agreement with the MD results. Differences are no doubt primarily due to applying the continuum concept of hardness to the atomic scale as well as the different ratios of the length scale governing the adhesion force to the geometrical dimensions of the hemisphere.

D. Influence of E/σ_Y on the separation modes

Based on the above results, $S=1.2$ is chosen as the brittle-ductile transition for $\delta_f/\delta_c=30$ in order to study the influence of E/σ_Y . This parameter was varied from 120 to 500. The value for μ was kept at 1.60 and the other material properties are summarized in Table III. It can be seen from both Figs. 4(a) and 4(b) that the loading curves coincide very closely, and the unloading curves show only a small difference. Hence, the parameter E/σ_Y does not affect the separation modes nearly as much as does S . In addition, we note that a large change of E/σ_Y only causes a small change of F_{adh}/F_f as predicted in Eq. (16).

E. Influence of μ on the separation modes

Table IV gives the material properties for studying the effect of μ and Fig. 5 shows the results. Similar to E/σ_Y , the parameter μ does not affect the separation mode significantly, but it does change F_{adh}/F_f substantially. From the combination of the KE model and the EKK model, the adherence force is inversely proportional to μ^3 , as shown in Eq.

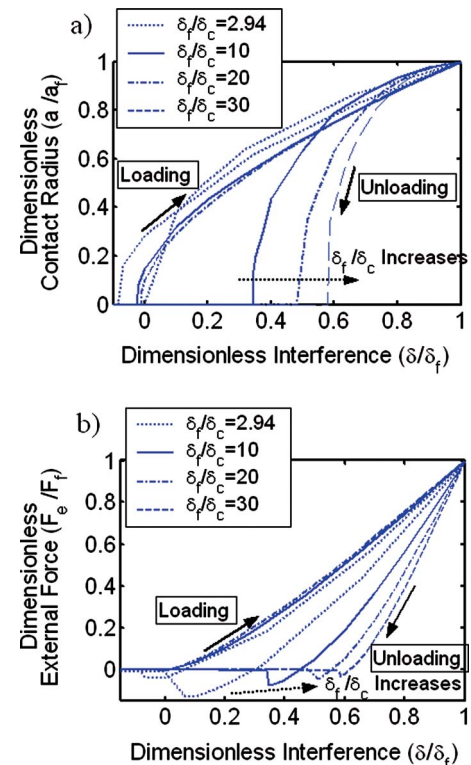


FIG. 6. (Color online) Dimensionless contact radius vs dimensionless interference (a) and dimensionless external force vs dimensionless interference (b) for a single load/unload cycle. The material properties and geometry are given as case 1 of Table V.

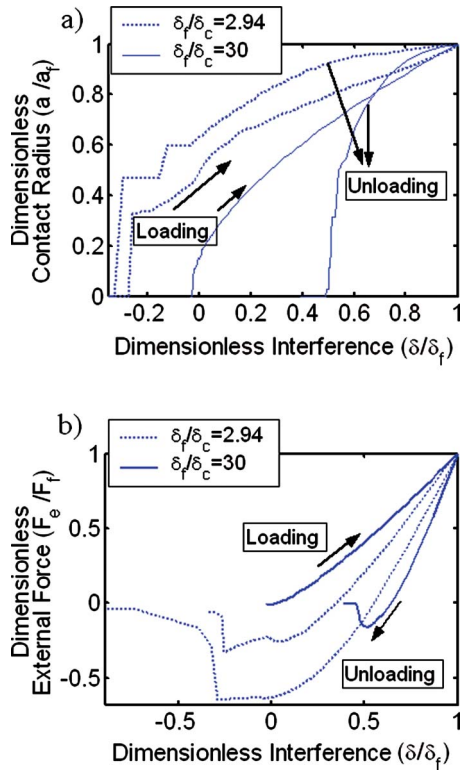


FIG. 7. (Color online) Dimensionless contact radius vs dimensionless interference (a) and dimensionless external force vs dimensionless interference (b) for a single load/unload cycle. The material properties and geometry are given as case 3 of Table V.

(16). The trend in this work is very close to this dependency if the separation is brittle. Note that in an elastic contact, greater adherence force also corresponds to smaller μ , but the dependence is weak.

F. Influence of δ_f/δ_c on the separation modes

The above simulations have shown that under the same large loading ($\delta_f/\delta_c=30$, so that the contact during maximum loading is mostly plastic), the parameter S has the greatest effect on the separation mode, while E/σ_Y and μ change the adherence force to a lesser degree. To study the influence of different loading levels, simulations at different load levels are performed with the four groups of material properties, respectively, listed in Table V which cover several combinations of S , E/σ_Y , and μ . The results are plotted in Figs. 6–8. In Fig. 6, the profiles of the curves are very similar and the separation is brittle under different loading levels with $S=0.6$. For $S=1.2$, the separations in both Figs. 7 and 8 are in the transition mode for $\delta_f/\delta_c=30$, but in the ductile mode for $\delta_f/\delta_c=2.94$. This behavior means that when S is near the brittle-ductile transition, δ_f/δ_c is another important factor for the occurrence of ductile separation. Lower δ_f/δ_c tends to cause ductile separation. This behavior, although counterintuitive, is qualitatively similar to both the MP and MJ models.

V. CONCLUSIONS

The impact of four parameters, i.e., S , E/σ_Y , μ , and the load level δ_f/δ_c on the separation modes of adhesive con-

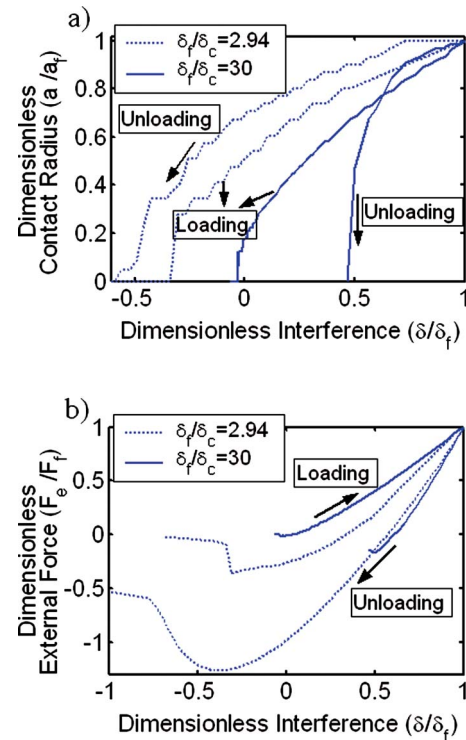


FIG. 8. (Color online) Dimensionless contact radius vs dimensionless interference (a) and dimensionless external force vs dimensionless interference (b) for a single load/unload cycle. The material properties and geometry are given as case 6 of Table V.

tacts, was investigated. The results show that S and δ_f/δ_c are the key parameters, while μ and E/σ_Y are less important. Ductile separation occurs when $S > 1.2$ for $\delta_f/\delta_c=30$, and the transition value of S is about 1.0 for a lower maximum loading interference (i.e., $\delta_f/\delta_c=2.94$). When S is near the transition, a smaller loading level can more readily cause ductile separation. The definition of ductile separation in this model is the occurrence of considerable stretch during unloading.

The results of this model are qualitatively consistent with two previous models, in that smaller loading and greater adhesion energy are more apt to cause ductile separation. However, there are quantitative differences with those models. The knowledge obtained in this work for the separation modes and for the dependence of the adherence force on the contact force, contact radius, and interference is of general interest in the understanding of adhesion and is also important for use by designers in a variety of single contact problems such as the contact in a micromechanical switch.

ACKNOWLEDGMENTS

This work was supported by DARPA under its S&T Fundamentals program through research contract HR0011-06-1-0051 to the University of California at San Diego with a subcontract to Northeastern University.

¹Y. Du, L. Chen, N. E. McGruer, G. G. Adams, and I. Etsion, *J. Colloid Interface Sci.* **312**, 522 (2007).

²N. E. McGruer, G. G. Adams, L. Chen, Z. J. Guo, and Y. Du, MEMS 2006, Istanbul, Turkey, 22–26 January 2006 (unpublished), p. 230.

³D. Maugis and H. M. Pollock, *Acta Metall.* **32**, 1323 (1984).

- ⁴S. K. Roy Chowdhury, N. E. W. Hartley, H. M. Pollock, and M. A. Wilkins, *J. Phys. D* **13**, 1761 (1980).
- ⁵D. Tabor, *J. Colloid Interface Sci.* **58**, 2 (1977).
- ⁶K. L. Johnson, K. Kendall, and A. D. Roberts, *Proc. R. Soc. London, Ser. A* **324**, 301 (1971).
- ⁷B. V. Derjaguin, V. M. Muller, and Y. P. Toporov, *J. Colloid Interface Sci.* **53**, 314 (1975).
- ⁸D. Maugis, *J. Colloid Interface Sci.* **150**, 243 (1992).
- ⁹W. R. Chang, I. Etsion, and D. B. Bogy, *J. Tribol.* **109**, 257 (1987).
- ¹⁰K. L. Johnson, *Contact Mechanics* (Cambridge University Press, Cambridge, UK, 1985).
- ¹¹S. Majumder, "Contact properties of a microelectromechanical switch with gold on-gold contacts," Ph.D thesis, Northeastern University, 2003.
- ¹²L. Kogut and I. Etsion, *J. Appl. Mech.* **69**, 657 (2002).
- ¹³L. Kogut and I. Etsion, *J. Colloid Interface Sci.* **261**, 372 (2003).
- ¹⁴K. L. Johnson, Proceedings of the Fourth IUTAM Congress, Amsterdam, North Holland, 1976 (unpublished), p. 133.
- ¹⁵S. Dj. Mesarovic and K. L. Johnson, *J. Mech. Phys. Solids* **48**, 2009 (2000).
- ¹⁶U. Landman, W. D. Luedtke, N. A. Burnham, and R. J. Colton, *Science* **248**, 454 (1990).
- ¹⁷J. Song and D. J. Srolovitz, *Acta Mater.* **54**, 5305 (2006).
- ¹⁸C. W. Yong, W. Smith, A. Dhir, and K. Kendall, *Tribol. Lett.* **26**, 235 (2007).
- ¹⁹J. R. Rice and R. M. Thomson, *Philos. Mag.* **29**, 73 (1974).
- ²⁰J. R. Rice, *J. Mech. Phys. Solids* **40**, 239 (1992).
- ²¹S. Majumder, N. E. McGruer, G. G. Adams, A. P. Zavracky, P. M. Zavracky, R. H. Morrison, and J. Krim, *Sens. Actuators, A* **93**, 19 (2001).
- ²²I. Etsion, Y. Kligerman, and Y. Kadin, *Int. J. Solids Struct.* **42**, 3716 (2005).
- ²³*Guide to Stability Design Criteria for Metal Structures*, 5th ed., edited by T. V. Galambos (Wiley, New York, 1998).